International Journal of Computational Methods
Vol. 7, No. 1 (2010) 191–214

DOI: 10.1142/S0219876210002131

A NOVEL GENERAL FORMULATION FOR SINGULAR STRESS FIELD USING THE ES-FEM METHOD FOR THE ANALYSIS OF MIXED-MODE CRACKS

G. R. LIU[*,†], N. NOURBAKHSHNIA[*,¶], L. CHEN[*] and Y. W. ZHANG[‡,§]

[*]*Center for Advanced Computations in Engineering Science (ACES),*
Department of Mechanical Engineering,
National University of Singapore,
9 Engineering Drive 1,
Singapore 117576, Singapore

[†]*Singapore-MIT Alliance (SMA), E4-04-10,*
4 Engineering Drive 3, Singapore, 117576, Singapore

[‡]*Department of Materials Science and Engineering,*
National University of Singapore, 7 Engineering Drive 1,
Singapore, 117574, Singapore

[§]*Large-scale Complex System, Programme,*
Institute of High Performance Computing,
1 Fusionopolis Way, Connexis,
Singapore 138632, Singapore
[¶]*nasibeh.n@nus.edu.sg.*

This paper presents a general formulation for simulating the singular stress field at the vicinity of the crack-tip for linear fracture mechanics problems, based on the edge-based smoothed finite element method (ES-FEM) settings. This novel "singular ES-FEM" makes use of the unique feature offered by the ES-FEM that only the assumed displacement values (not the derivatives) are required to compute the stiffness matrix of the discretized system. The present singular ES-FEM method uses a basic mesh of linear triangular elements and a layer of novel "five-noded crack-tip elements" sharing the crack-tip node. The five-noded crack-tip element has one additional node on each of the edges connected to the crack-tip, and the locations of the "edge-node" can be arbitrary. A number of examples are analyzed and the results demonstrate that the present singular ES-FEM is generally softer and much more accurate than the existing FEM. The stress intensity factors obtained using the singular ES-FEM are very stable for different area-integration paths designed around the crack-tip. The present singular ES-FEM is found an excellent alternative to the standard FEM for fracture problems.

Keywords: Mesh free method; smoothed finite element method, singular smoothed finite element method, mixed mode crack problems.

[¶]Corresponding author.

1. Introduction

The strain smoothing technique was used for stabilizing the solutions of the nodal integrated meshfree methods [Chen *et al.* (2000)], and it was also applied in the natural element method [Yoo *et al.* (2004)]. The strain smoothing technique was later implemented to the finite element method (FEM) settings, and the smoothed finite element method (SFEM) was developed using cell-based smoothing domains (SDs) created by further dividing the elements [Liu *et al.* (2007a)]. Such a cell-based smoothed FEM (or CS-FEM) has a number of important properties [Liu *et al.* (2007b)] and works naturally well for heavily distorted elements and the general n-sided polygonal elements [Dai *et al.* (2007)]. A node-based smoothed finite element method (NS-FEM) [Liu *et al.* (2009c)] was also proposed using SDs constructed based on nodes in FEM settings. When triangular elements are used, the NS-FEM gives the same results as the node-based uniform strain elements [Dohrmann *et al.* (2000)] or the LC-PIM [Liu *et al.* (2005)] using linear shape functions for interpolation. Similar to other nodal integrated methods [Puso and Solberg (2006); Puso *et al.* 2008; Nagashima (1999)]; NS-FEM suffers from the temporal instability due to its "overly soft" feature rooted at the use of a relatively small number of SDs in relation to the nodes [Liu (2008)]. Liu *et al.* [2009a] formulated then the edge-based smoothed finite element method (ES-FEM) to eliminate this temporal instability. The ES-FEM works very well with triangular elements and exhibits super convergence properties, in addition to its ultra accuracy: it can be more accurate even compared to the FEM using quadrilateral elements with the same set of nodes. The ES-FEM was found computationally very efficient [Chen *et al.* (2009)], and known as the "star performer" among all the linear numerical models [Liu (2009)]. Most importantly, in the framework of ES-FEM formulation, stiffness matrix calculation requires only evaluating the shape functions values (and not the derivatives) on the boundaries of the strain SDs associated with the element edges. Making use of this significant property, displacement fields can enriched with a desired order of $\sqrt{r}$ for linear fracture problems [Liu *et al.* (2009b)] using the simple and "nonmapping" point interpolation method (PIM) [Liu (2009)]. As a result, a proper singular stress field can be perfectly produced in the vicinity of the crack-tip, without using any mapping procedure.

In this paper, we provide a general formulation for fracture problems based on the ES-FEM approach using a base mesh of linear triangular elements that can be automatically generated for complicated geometries. In the present singular ES-FEM, we use one layer of "five-noded crack-tip elements" specially designed for simulating the stress and strain singularity near the crack-tip. The five-noded crack-tip element has one additional node on each of the edges connected to the crack-tip, and the locations of the "edge-node" can be arbitrary. Therefore, the formulation is quite general and straightforward. To evaluate the stress intensity factors, we use the interaction integral method widely used in the FEM. Numerical examples will be presented to examine the performance of the singular ES-FEM, in comparison with other existing FEM models. The numerical results in terms of strain energy and stress intensity factors have shown clearly that the present singular ES-FEM method is much more accurate than the standard FEM and even the ES-FEM with the same mesh. Moreover, the singular ES-FEM works very well with the interaction integral method and produces stable and path-independent results in terms of stress intensity factors for the mixed-mode fracture problems.

This paper is outlined as follows. In Sec. 2, the idea of the singular ES-FEM is introduced and a general procedure for creating the shape functions with proper singularity near the crack-tip is proposed. We then present the approach to compute the stiffness matrix, especially for the layer of the five-noded crack-tip elements. In Sec. 3, the accuracy of the present method is analyzed using numerical examples and comparisons are made between our singular ES-FEM and standard ES-FEM-T3 and FEM-T3. Finally, some conclusions are drawn in Sec. 4.

2. A General Formulation of Singular ES-FEM

2.1. *Reproducing stress singularity at the crack-tip*

2.1.1. *Displacement interpolation along the element edge*

When a linear fracture mechanics problem is simulated using a numerical approach, the singular stress field near the crack-tip should be properly simulated. In the FEM, the most widely used technique to simulate this kind of stress singularity is the so-called (quadratic) six-node crack-tip element in which the mid-edge nodes are shifted by a quarter edge-lengths towards the crack-tip. The singularity is then achieved nicely by the well-known isoparametric mapping procedure [Liu and Quek (2003); Zienkiewicz and Taylor (2007)].

In the present singular ES-FEM method, we use the simple “nonmapping” PIM method [Liu *et al.* (2009)] for displacement field construction, because only the shape function values (not the derivatives) are required in the ES-FEM formulation [Liu *et al.* (2009a)]. Making use of this important feature of the ES-FEM, the stress singularity at the crack-tip can be easily enriched with extra basis functions of proper fractional order polynomials. Figure 1 shows a singular ES-FEM model for a fracture problem with a horizontal opening crack, where we add in a node on each edge of the triangular elements connected to the crack-tip node, as shown in Fig. 2(a). The location of the added intermediate node can be in general at any point on the edge, as shown in Fig. 2(b). The displacement field, for example, the component u, at any point of interest on an edge directly connected to the crack-tip can be approximated using:

$$u = c_0 + c_1 r + c_2 \sqrt{r}, \tag{1}$$

where r is the radial coordinate originated at the crack-tip (node 1), and c_i ($i = 0, 1, 2$) are the constants yet to be determined. Clearly, the assumed displacement using Eq. (1) is at least linearly complete. Using Eq. (1), the displacements at node

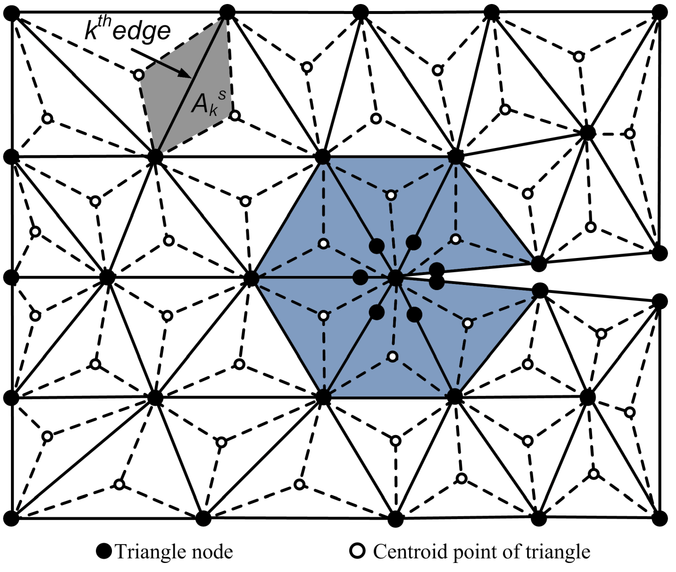

Fig. 1. An ES-FEM model: Triangular elements mesh (solid lines), quadrilateral smoothing domains (dashed lines) for a fracture problem with an opening crack.

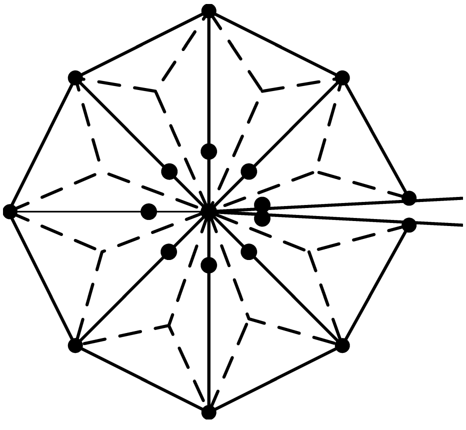

(a) An additional node is added on each edge of the triangular elements connected to the crack-tip.

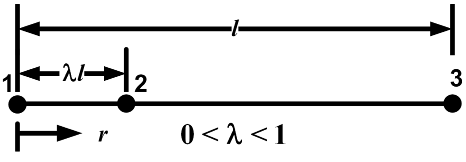

(b) coordinate for an edge connected to the crack-tip

Fig. 2. Node arrangement near the crack-tip. Dash lines show the boundary of a smoothing domain for an edge directly connected to the crack-tip node.

1, 2, and 3 can be expressed as:

$$u_1 = c_0; \quad (r = 0 \text{ at node } 1), \tag{2}$$

$$u_2 = c_0 + c_1\lambda l + c_2\sqrt{\lambda l}; \quad (r = \lambda l \text{ at node } 2), \tag{3}$$

$$u_3 = c_0 + c_1 l + c_2\sqrt{l}; \quad (r = l \text{ at node } 3), \tag{4}$$

where u_i $(i = 1, 2, 3)$ are the nodal displacements, l is the length of the element edge, and $\lambda \in (0\ \ 1)$ controls the location of node 2. Solving this simultaneous system of three Eqs. (2)–(4) for c_i, we shall have:

$$\begin{cases} c_0 = u_1, \\ c_1 = \dfrac{1}{\lambda l}\left[\left(-1 + \dfrac{(1-\lambda)\sqrt{\lambda l}}{\sqrt{\lambda l} - \lambda\sqrt{l}}\right)u_1 + \left(1 - \dfrac{\sqrt{\lambda l}}{\sqrt{\lambda l} - \lambda\sqrt{l}}\right)u_2 + \dfrac{\lambda\sqrt{\lambda l}}{\sqrt{\lambda l} - \lambda\sqrt{l}}u_3\right], \\ c_2 = \dfrac{1}{\sqrt{\lambda l} - \lambda\sqrt{l}}[(\lambda - 1)u_1 + u_2 - \lambda u_3]. \end{cases} \tag{5}$$

After substituting c_i $(i = 1, 2, 3)$ back to Eq. (1), we obtain:

$$u = \begin{Bmatrix} \underbrace{1 + \dfrac{r}{\lambda l}\left(-1 + \dfrac{(1-\lambda)\sqrt{\lambda l}}{\sqrt{\lambda l} - \lambda\sqrt{l}}\right) + \dfrac{\sqrt{r}}{\sqrt{\lambda l} - \lambda\sqrt{l}}(\lambda - 1)}_{\phi_1} \\ \underbrace{\dfrac{r}{\lambda l}\left(1 - \dfrac{\sqrt{\lambda l}}{\sqrt{\lambda l} - \lambda\sqrt{l}}\right) + \dfrac{\sqrt{r}}{\sqrt{\lambda l} - \lambda\sqrt{l}}}_{\phi_2} \\ \underbrace{\dfrac{r}{\lambda l}\left(\dfrac{\lambda\sqrt{\lambda l}}{\sqrt{\lambda l} - \lambda\sqrt{l}}\right) - \dfrac{\lambda\sqrt{r}}{\sqrt{\lambda l} - \lambda\sqrt{l}}}_{\phi_3} \end{Bmatrix}^T \begin{Bmatrix} u_1 \\ u_2 \\ u_3 \end{Bmatrix}, \tag{6}$$

where ϕ_i $(i = 1, 2, 3)$ are the basic nodal shape functions for these three nodes on the edge connected to the crack-tip that can be written in the following row-matrix form:

$$\Phi = \begin{Bmatrix} \underbrace{1 + \dfrac{r}{\lambda l}\left(-1 + \dfrac{(1-\lambda)\sqrt{\lambda l}}{\sqrt{\lambda l} - \lambda\sqrt{l}}\right) + \dfrac{\sqrt{r}}{\sqrt{\lambda l} - \lambda\sqrt{l}}(\lambda - 1)}_{\phi_1} \\ \underbrace{\dfrac{r}{\lambda l}\left(1 - \dfrac{\sqrt{\lambda l}}{\sqrt{\lambda l} - \lambda\sqrt{l}}\right) + \dfrac{\sqrt{r}}{\sqrt{\lambda l} - \lambda\sqrt{l}}}_{\phi_2} \\ \underbrace{\dfrac{r}{\lambda l}\left(\dfrac{\lambda\sqrt{\lambda l}}{\sqrt{\lambda l} - \lambda\sqrt{l}}\right) - \dfrac{\lambda\sqrt{r}}{\sqrt{\lambda l} - \lambda\sqrt{l}}}_{\phi_3} \end{Bmatrix}^T, \tag{7}$$

where

$$\begin{cases} \phi_1 = 1 + \dfrac{r}{\lambda l}\left(-1 + \dfrac{(1-\lambda)\sqrt{\lambda l}}{\sqrt{\lambda l} - \lambda\sqrt{l}}\right) + \dfrac{\sqrt{r}}{\sqrt{\lambda l} - \lambda\sqrt{l}}(\lambda - 1), \\ \phi_2 = \dfrac{r}{\lambda l}\left(1 - \dfrac{\sqrt{\lambda l}}{\sqrt{\lambda l} - \lambda\sqrt{l}}\right) + \dfrac{\sqrt{r}}{\sqrt{\lambda l} - \lambda\sqrt{l}}, \\ \phi_3 = \dfrac{r}{\lambda l}\left(\dfrac{\lambda\sqrt{\lambda l}}{\sqrt{\lambda l} - \lambda\sqrt{l}}\right) - \dfrac{\lambda\sqrt{r}}{\sqrt{\lambda l} - \lambda\sqrt{l}}. \end{cases} \tag{8}$$

It is clear that the shape functions are (complete) linear in r and "enriched" with $\sqrt{r}$ that is capable of producing a strain (hence stress) singularity field of an order of 1/2 near the crack-tip, because the strain is evaluated from the derivatives of the assumed displacements. Note also that in our formulation, the intermediate edge-node can be at any position on the edge controlled by factor λ, which is very general and different from the usual FEM crack-tip elements where the intermediate nodes are located at a quarter of lengths to the crack-tip. Moreover, the usual FEM crack-tip element achieves the singularity by coordinate mapping, while the singular ES-FEM achieves the singularity via direct interpolation with a proper fractional order basis term and no mapping is needed.

2.1.2. *Displacement interpolation within a crack-tip element*

In the present ES-FEM, we use a base mesh of three-node linear triangle elements for areas without singularity, and one layer of the specially designed singular five-noded triangular elements containing the crack-tip to produce the desired stress singularity behavior at the crack-tip, as shown in Fig. 3. The same procedure of

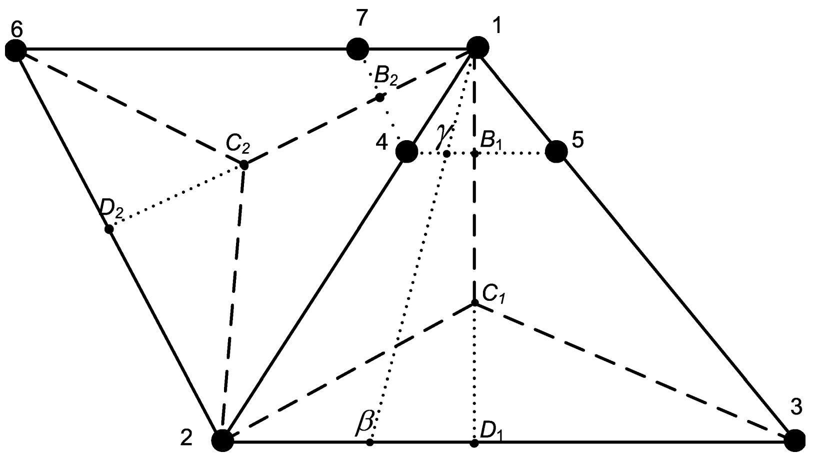

Fig. 3. Two five-node elements connected to the crack-tip node 1.

producing the stress singularity of an order of 1/2 near the crack-tip along the element edge described in Sec. 2.1.1 can be properly developed within a crack-tip element. The procedure follows that presented in Liu *et al.* [2009b], but using the basic nodal shape functions for nodes at an edge given in Eq. (8).

We first assume that in the radial directions originated from the crack-tip, the displacements vary in the same fashion as given in Eq. (1). In the tangential direction, however, it is assumed to vary linearly. This assumption ensures the compatibility along the edges between the three-node linear triangular elements and the five-node crack-tip elements. Figure 3 shows two five-node elements, parts of which form one edge-based SD. The points D_1 and B_1 in this figure are, respectively, the midpoints of lines 2–3 and 4–5. The displacements at these two points can be evaluated simply by averaging (because of linear variation assumption on the tangential direction):

$$u_{B_1} = \frac{1}{2}(u_4 + u_5), \tag{9}$$

$$u_{D_1} = \frac{1}{2}(u_2 + u_3). \tag{10}$$

At any point on the line $1 - B_1 - D_1$ displacement is then evaluated using the shape functions for edges given in Eq. (8):

$$u = u_1\phi_1 + u_{B_1}\phi_2 + u_{D_1}\phi_3. \tag{11}$$

Substituting Eqs. (9) and (10) into Eq. (11), we have:

$$u = u_1\phi_1 + \frac{1}{2}(u_4 + u_5)\phi_2 + \frac{1}{2}(u_2 + u_3)\phi_3. \tag{12}$$

Hence, the interpolation at any point on line $1 - B_1 - D_1$, can be given as follows:

$$u = u_1\phi_1 + \frac{1}{2}\phi_3 u_2 + \frac{1}{2}\phi_3 u_3 + \frac{1}{2}\phi_2 u_4 + \frac{1}{2}\phi_2 u_5. \tag{13}$$

Similarly, at any point on line $1 - \gamma - \beta$ (see, Fig. 3), the displacement can be calculated as

$$u = u_1\phi_1 + u_\gamma\phi_2 + u_\beta\phi_3, \tag{14}$$

where

$$u_\gamma = \left(1 - \frac{l_{\gamma-4}}{l_{4-5}}\right) u_4 + \frac{l_{\gamma-4}}{l_{4-5}} u_5, \tag{15}$$

$$u_\beta = \left(1 - \frac{l_{\beta-2}}{l_{2-3}}\right) u_2 + \frac{l_{\beta-2}}{l_{2-3}} u_3, \tag{16}$$

in which l_{i-j} is the distance between points i and j. Because the simple fact that $\frac{l_{\gamma-4}}{l_{4-5}} = \frac{l_{\beta-2}}{l_{2-3}} = \alpha$, we finally arrive at

$$u = \underbrace{\phi_1}_{N_1} u_1 + \underbrace{(1-\alpha)\phi_3}_{N_2} u_2 + \underbrace{\alpha\phi_3}_{N_3} u_3 + \underbrace{(1-\alpha)\phi_2}_{N_4} u_4 + \underbrace{\alpha\phi_2}_{N_5} u_5. \tag{17}$$

The general form of the nodal shape functions for the interpolation at any point within the five-node crack-tip element can be written as:

$$\begin{cases} N_1 = 1 + \dfrac{r}{\lambda l}\left(-1 + \dfrac{(1-\lambda)\sqrt{\lambda l}}{\sqrt{\lambda l} - \lambda\sqrt{l}}\right) + \dfrac{\sqrt{r}}{\sqrt{\lambda l} - \lambda\sqrt{l}}(\lambda - 1), \\ N_2 = (1-\alpha)\left(\dfrac{r}{\lambda l}\left(\dfrac{\lambda\sqrt{\lambda l}}{\sqrt{\lambda l} - \lambda\sqrt{l}}\right) - \dfrac{\lambda\sqrt{r}}{\sqrt{\lambda l} - \lambda\sqrt{l}}\right), \\ N_3 = \alpha\left(\dfrac{r}{\lambda l}\left(\dfrac{\lambda\sqrt{\lambda l}}{\sqrt{\lambda l} - \lambda\sqrt{l}}\right) - \dfrac{\lambda\sqrt{r}}{\sqrt{\lambda l} - \lambda\sqrt{l}}\right), \\ N_4 = (1-\alpha)\left(\dfrac{r}{\lambda l}\left(1 - \dfrac{\sqrt{\lambda l}}{\sqrt{\lambda l} - \lambda\sqrt{l}}\right) + \dfrac{\sqrt{r}}{\sqrt{\lambda l} - \lambda\sqrt{l}}\right), \\ N_5 = \alpha\left(\dfrac{r}{\lambda l}\left(1 - \dfrac{\sqrt{\lambda l}}{\sqrt{\lambda l} - \lambda\sqrt{l}}\right) + \dfrac{\sqrt{r}}{\sqrt{\lambda l} - \lambda\sqrt{l}}\right). \end{cases} \tag{18}$$

Because in our singular ES-FEM, we do not need derivatives of shape functions, Eq. (18) is all we need in computing the stiffness matrix for creating our numerical model.

2.2. *Strain smoothing domains associated with the edges*

In order to calculate the stiffness matrix in the present ES-FEM, strain SDs are constructed associated with the edges of each element. Each three-node triangular elements are divided into three equal sub-triangular areas each of which has one edge of the element as the base, and they all share the center of the element as a vertex. Two such sub-triangular areas sharing with the same edge form a SD, as shown in Fig. 4(a). For a five-node crack-tip element, however, we can increase the number of sub-smoothing domains (S-SDs) associated with the edges directly connected to the crack-tip node for better capturing the singularity field. Figure 4 shows three cases of one, two, and three S-SDs per edge for the five-node crack-tip elements. The effects of the use of different numbers of S-SDs will be examined in the example section.

2.3. *Stiffness matrix evaluation*

Based on the ES-FEM procedure [Liu *et al.* (2009a)], the entries of the global stiffness matrix of the whole model can be calculated by

$$\overline{\mathbf{K}}_{IJ} = \sum_{k=1}^{N_s} \overline{\mathbf{K}}_{IJ,k}, \tag{19}$$

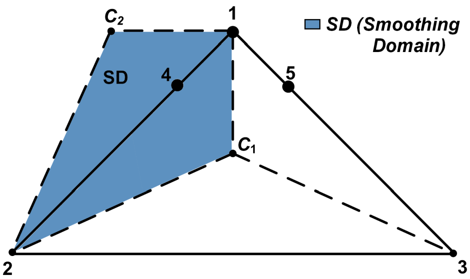

(a) One smoothing domain 1-C1-2-C2-1 for one edge 1-2 ($SD = 1$)

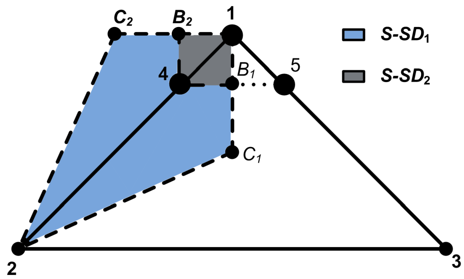

(b) Two sub-smoothing domains: 1-B1-4-B2-1 and 4-B1-C1-2-C2-B2-4 for one crack-tip edge 1-2 (S-$SD = 2$)

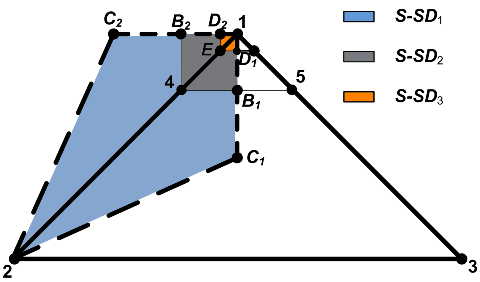

(c) Three sub-smoothing domains: 1-D1-E-D2-1, E-D1-B1-4-B2-D2-E, 4-B1-C1-2-C2-B2-4 for one crack-tip edge (S-$SD = 3$)

Fig. 4. Division of the smoothing domain associated with edge 1-2 into smoothing domains. For crack-tip edges, we may use SD = 1, 2, or 3. For other edges, we use SD = 1.

where $\bar{\mathrm{K}}_{IJ}$ is the IJth entry of the global stiffness matrix and $\bar{\mathrm{K}}_{IJ,k}$ is that of the stiffness matrix of the kth SD, and N_s is the total number of SDs. $\bar{\mathrm{K}}_{IJ,k}$ can also be computed by [Liu *et al.* (2009a)]

$$\overline{\mathbf{K}}_{IJ,k} = \int_{A_k^s} \overline{\mathbf{B}}_I^T \mathbf{D} \overline{\mathbf{B}}_J dA, \tag{20}$$

in which A_k^s is the strain smoothing area associated with edge k. The smoothed strain matrix $\bar{\mathbf{B}}_I^T$ has the form of

$$\overline{\mathbf{B}}_I(x_k) = \begin{bmatrix} \bar{b}_{Ix}(x_k) & 0 \\ 0 & \bar{b}_{Iy}(x_k) \\ \bar{b}_{Iy}(x_k) & \bar{b}_{Ix}(x_k) \end{bmatrix}, \tag{21}$$

where

$$\bar{b}_{Ih}(x_k) = \frac{1}{A_k^s} \int_{\Gamma_k^s} N_I(x) n_h^k(x) d\Gamma; \quad (h = x, y), \tag{22}$$

in which N_I is the shape functions obtained for the element housing x, Γ_k^s is the boundary of the SD, and n_h^k is the hth component of the outward normal vector on the boundary Γ_k^s. Numerically, Eq. (22) can be calculated by

$$\bar{b}_{Ih}(x_k) = \frac{1}{A_k^s} \sum_{i=1}^{M} \sum_{j=1}^{N\text{gp}} N_I(x_{i,j}^{\text{GP}}) w_{i,j}^{\text{GP}} n_{ih}^k; \quad (h = x, y), \tag{23}$$

where M is the number of (line) boundary segments of Γ_k^s, $x_{i,j}^{\text{GP}}$ is the Gaussian point location on the ith boundary segment, $w_{i,j}^{\text{GP}}$ is the Gaussian weight associated with the Gaussian point $x_{i,j}^{\text{GP}}$, Ngp is the number of Gaussian points on the ith boundary segment, and n_{ih}^k is the hth component of the unit outward vector on the ith boundary segment.

It should be noticed that for the boundary segments associated with the standard three-node triangular elements, one Gaussian point at the midpoint of the (line) boundary segment is sufficient, due to the linear interpolation used. For a five-node crack-tip element, however, more Gaussian points should be used, because the shape functions are no longer linear on the segment. In addition, for a five-node crack-tip element each SD can be divided into more S-SDs, for instance S-SD$_1$, S-SD$_2$, and S-SD$_3$ shown in Fig. 4. In such a case, the SD's boundary segments which are directly connected to the crack-tip have been divided into more sub-segments and integration should be evaluated along each sub-segment with more than one Gauss points. For example, as shown in Fig. 4(c), the boundary segment $1 - C_1$ has been divided into three sub-segments $1 - D_1$, $D_1 - B_1$, and $B_1 - C_1$, and boundary segment $1 - C_2$ has also been divided into three sub-segments $1 - D_2$, $D_2 - B_2$, and $B_2 - C_2$. In the numerical example section, we will show that the use of proper number of subdivisions can improve the accuracy of the results.

2.4. *J-integral and stress intensity factor evaluation*

2.4.1. *General formulations*

Under the assumption of small displacement gradient, the standard J-integral for a two-dimensional, planar, elastic solid including a sharp crack is defined in the form of line-path integration by [Rice (1968)]:

$$J = -\int_{\Gamma_J} \left(\sigma_{ij} \frac{\partial u_i}{\partial x_1} - w\delta_{1j} \right) n_j d\Gamma, \tag{24}$$

where Γ_J is an arbitrary line-path enclosing the crack-tip located at the origin of the coordinate system as shown in Fig. 5(a), n_j is the outward unit normal on Γ_J, σ_{ij} the stress, u_i the displacement vector referred to a Cartesian coordinate system,

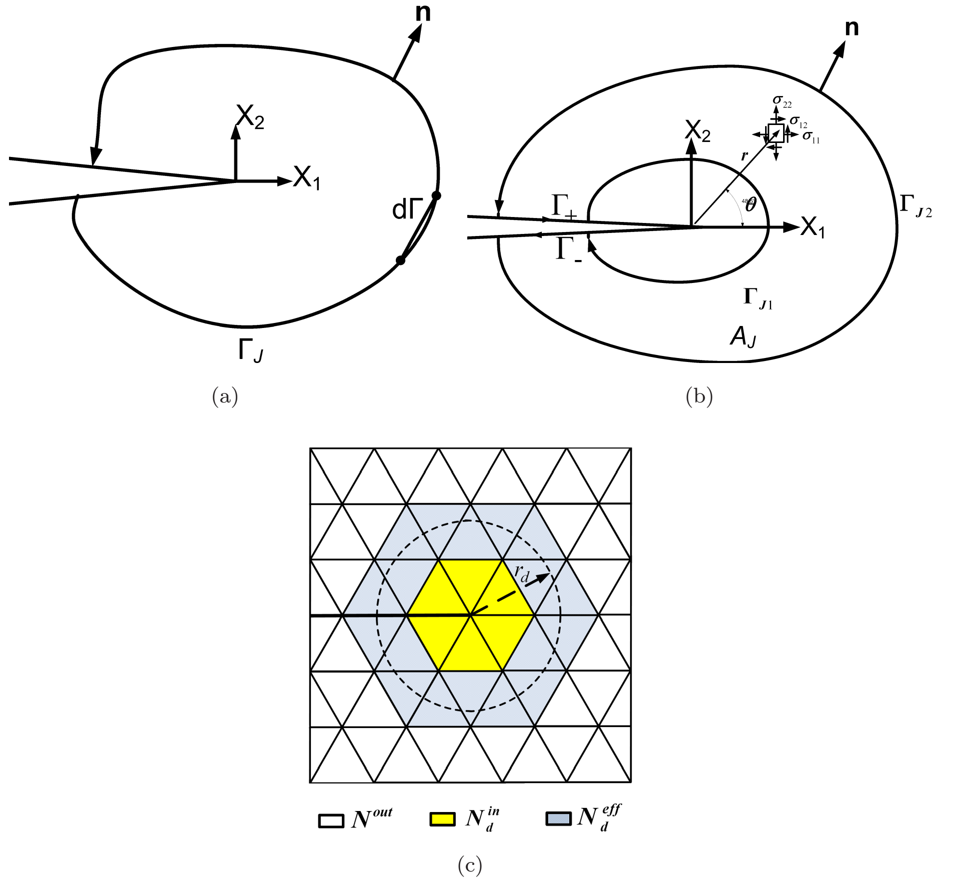

Fig. 5. Typical types of closed paths around the crack-tip: (a) line-path; (b) area-path; (c) A typical method to select elements around the crack-tip to form the area-path for the calculation of the interaction integral.

and w the strain energy density. Theoretically, we know that J value is integration path-independent. Numerically, however, we often observe path dependence.

To achieve better "numerically" path independency, we often use a so-called area–path in lieu of the line-path for the integration. To obtain such an area–path integration formula, the integrand in Eq. (24) is multiplied with a smoothing weighting function q as [Li *et al.* (1985)]:

$$J = -\int_{\Gamma_J} \left(\sigma_{ij} \frac{\partial u_i}{\partial x_1} - w\delta_{1j} \right) n_j q d\Gamma. \tag{25}$$

Consider a typical two-dimensional sharp-cracked body with an assumed closed contour Γ_J around its crack-tip as shown in Fig. 5(b), where we have $\Gamma_J = \Gamma_{J1} \cup \Gamma_- \cup \Gamma_{J2} \cup \Gamma_+$. The area A_J is enclosed by line segments Γ_{J1}, Γ_-, Γ_{J2} and Γ_+. The segments Γ_- and Γ_+ are, respectively, the boundaries of the lower and upper crack face. For such a closed contour, J-integral can now be defined in the form of area-integration by [Li *et al.* (1985)]:

$$J = \int_{A_J} \left(\sigma_{ij} \frac{\partial u_i}{\partial x_1} - w\delta_{1j} \right) \frac{\partial q}{\partial x_j} dA, \tag{26}$$

where δ_{1j} is the Kronecker delta and q is now a sufficiently smoothing function defined on A_J. We will discuss in Sec. 2.4.2 on how q should be defined for our ES-FEM model.

In order to evaluate the stress intensity factors for mixed modes effectively, the method of area-path interaction integral [Yau *et al.* (1980); Shih and Asaro (1985)] will be used in this paper by calculating the following integration first.

$$I^{(1,2)} = -\int_{A_J} \left[w^{(1,2)}\delta_{1j} - \sigma_{ij}^{(1)} \frac{\partial u_i^{(2)}}{\partial x_1} - \sigma_{ij}^{(2)} \frac{\partial u_i^{(1)}}{\partial x_1} \right] \frac{\partial q}{\partial x_j} dA. \tag{27}$$

The stress intensity factors can be evaluated then as

$$\begin{cases} K_I^{(1)} = \dfrac{2}{E^*} I^{(1,\text{Mode } I)}, \\ K_{II}^{(1)} = \dfrac{2}{E^*} I^{(1,\text{Mode } II)}, \end{cases} \tag{28}$$

where E^* is defined in terms of material parameters E (Young's modulus) and ν (Poisson's ratio) as Eq. (29):

$$E^* = \begin{cases} E & \text{plane stress,} \\ \dfrac{E}{1-\nu^2} & \text{plane strain.} \end{cases} \tag{29}$$

2.4.2. *Determination of area-path*

Because the ES-FEM uses a basic mesh of linear three-node triangular elements, a simple scheme can be devised to determine the area-path A_J shown in Fig. 5(c). First, a set of elements having at least one node within a circle of radius r_d is found, and this element set is denoted as N_d. The weighting function q is then chosen as a piecewise linear function passing through the nodal values at all the nodes belonging to all the elements in N_d. If a node n_i belonging to an element $e \in N_d$ lies outside the circle, then the nodal value of the weighting function is set to zero: $q_i = 0$; if a node n_i lies inside the circle, the weighting function is then set to unit: $q_i = 1$. Since the elements set N_d^{in} has all the nodes inside the circle as shown in Fig. 5(c), the weight function will be a constant (unit) within all these elements in set N_d^{in}. Because the gradient of q is used in Eq. (27) the element set N_d^{in} will contribute nothing to the interaction integral. The nonzero contribution to the integral is obtained only for elements set N_d^{eff} with (two) edges intersecting the circle. Because three-node elements are used in ES-FEM, any circle will naturally always select a layer of elements that form A_J.

3. Numerical Examples

In this section, some examples are presented to demonstrate the accuracy and stability of singular ES-FEM, for linear elastic fracture mechanics problems. All the problems have been solved using FEM-T3, standard ES-FEM, and Singular ES-FEM, using the same basic mesh of linear triangular elements. The effect of the number of S-SDs in the Singular ES-FEM has been also examined in the examples. In addition, the effects of different values of λ that changes the intermediate node locations on the edges connecting to the crack-tip node is also investigated in details using the first example problem.

3.1. *Rectangular finite plate with a central crack under pure mode I*

A rectangular finite plate containing a central crack is first analyzed under tension load at its top edge. This problem is of pure mode I. the structure is depicted in Fig. 6, and the parameters used are $w = 10.0\,\text{cm}$, $L = 25.0\,\text{cm}$, $a = 4\,\text{cm}$, and $\sigma = 1\,\text{N/cm}^2$. The material is isotropic elastic and material constants are $E = 3 \times 10^7\,\text{N/cm}^2$ and $\nu = 0.25$. The analytical solution of stress intensity factors for such a structure is given by Tada *et al.* [2000].

$$K_I = \sigma\sqrt{\pi a}\left[1 - 0.025\left(\frac{a}{w}\right)^2 - 0.06\left(\frac{a}{w}\right)^4\right]\left(\sec\left(\frac{\pi a}{2w}\right)\right)^{0.5}. \tag{30}$$

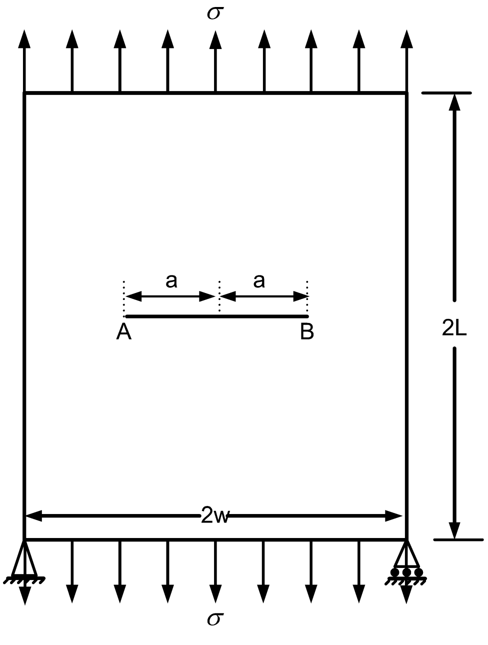

Fig. 6. Homogenous finite plate with a central crack under tension (pure mode I).

The problem is then solved using FEM-T3, ES-FEM, and the present Singular ES-FEM. In the singular ES-FEM, we used one SD (SD = 1) and two cases of one and two S-SDs (S-SD = 1 and S-SD = 2) for the crack-tip elements. In addition, for the case of using two S-SDs, the effects of the intermediate node position on the crack-tip edges have been examined by choosing different values of λ. The results in term of both the strain energy and stress intensity factors at each crack-tip are illustrated in Figs. 7–9. From these results, it can be seen that:

(1) The strain energy results of the present singular ES-FEM are much more accurate and convergence much faster than the FEM-T3 and standard ES-FEM.
(2) Singular ES-FEM with SD = 1 works very well in this example to evaluate the stress intensity factors at either of two crack-tip points.
(3) The results related to cases of different λ shows that the place of intermediate nodes does not significantly affect on the results. As a conclusion, based on our singular ES-FEM formulation, we do not have to place the intermediate node at one-quarter edge length as in the quadratic FEM elements.
(4) Figures 8 and 9 show that the value of stress intensity factors and related numerical error at crack-tips A and B are very close to each other and almost the same. This expected result confirms that our method works very well for the domains including more than one crack.
(5) Increasing the number of S-SDs somewhat improve the results, however, the improvement is not too much in this example especially for the finer meshes.

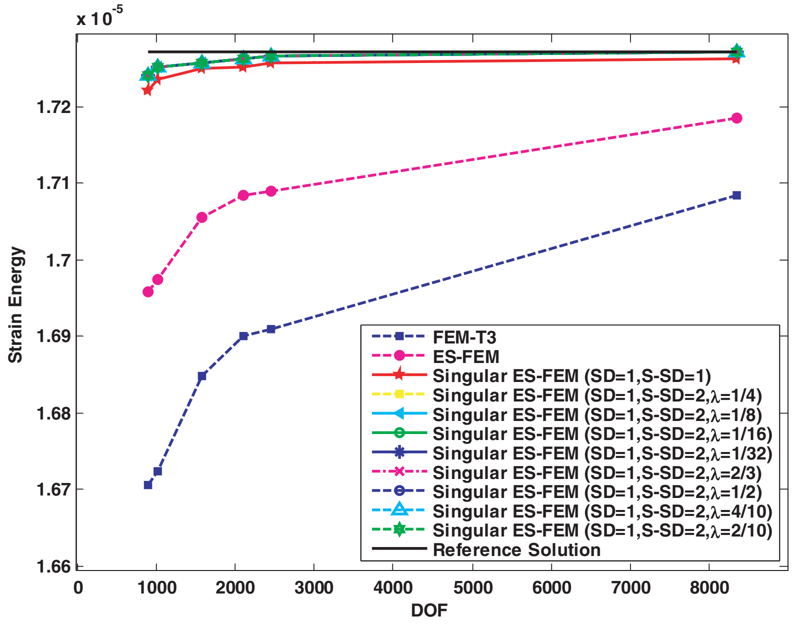

Fig. 7. Strain energy results for the finite plate under mode I.

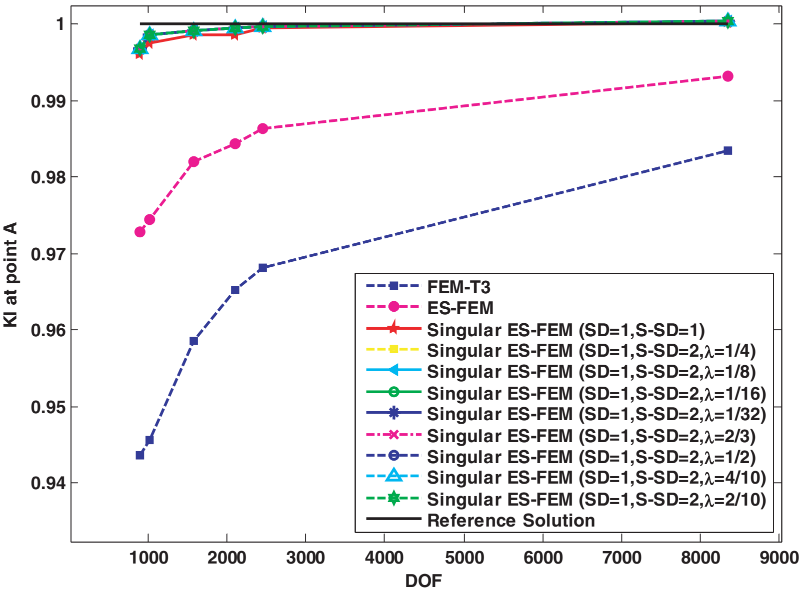

Fig. 8. Normalized stress intensity factor at point A for the finite plate under mode I.

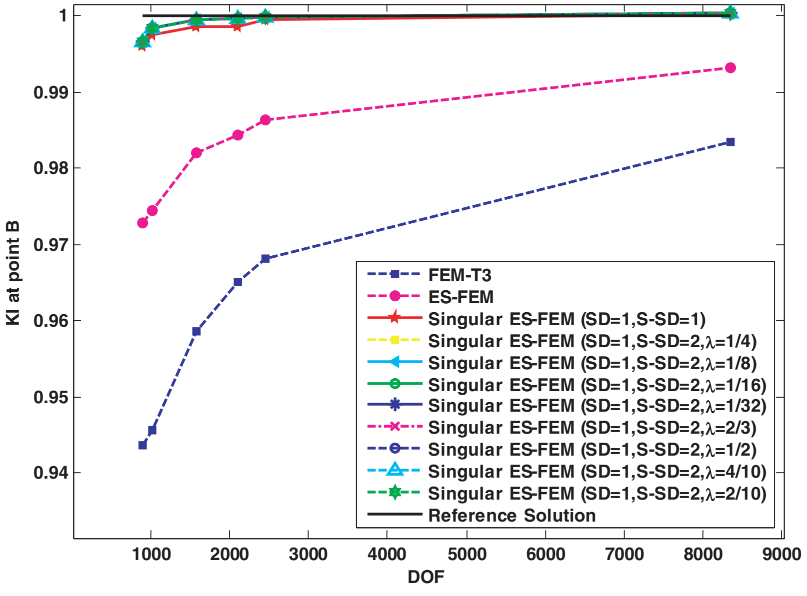

Fig. 9. Normalized stress intensity factor at point B for the finite plate under mode I.

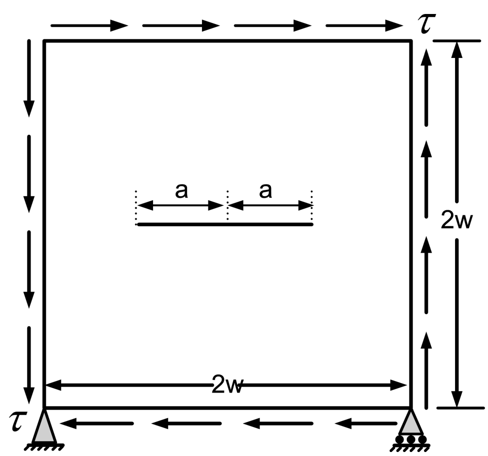

Fig. 10. Infinite plate with a central crack under pure mode II.

3.2. *Homogeneous infinite plate with a central crack under pure mode II*

In this example, we study the homogeneous infinite plate with the similar geometry but under the pure shear mode. This structure has been shown in Fig. 10. The analytical solution for this plate when its dimensions goes to infinitive is valid and the stress intensity factor in mode II equals to $K_{\rm II} = \tau\sqrt{\pi a}$, in which τ is the shear stress and a is half of the crack length. In this example, the plate dimensions has been fixed as $a = 10$ mm and $w = 200$ mm, and since $w/a = 20$, the solution for the infinite plate with a central crack can be employed. The problem has been solved under pure shear mode using different methods including FEM-T3, ES-FEM, and Singular ES-FEM. The results in term of strain energy and stress intensity factor have been tabulated in Tables 1–3 and depicted in Figs. 11 and 12. Similar to the previous example and regarding to the results tabulated in the tables it can be seen that the value of stress intensity factor at points A and B is very close to each other. Therefore, the stress intensity factor behavior has been plotted only for one of the crack-tip points. Based on the results it can be clearly observed that:

(1) Singular ES-FEM with SD = 1 works very well in this example to evaluate the strain energy and stress intensity factors at either of two crack-tip points.
(2) Based on Tables 2 and 3 it can be clearly observed that by increasing the mesh the value of error declines to 0.02% for Singular ES-FEM. It is much more less in comparison with FEM and standard ES-FEM.

3.3. *Double edge crack specimen*

The geometry of double edge crack specimen is shown in Fig. 13. The specimen is subjected to a remoter tensile stress σ at top edge and being fixed at the bottom.

Table 1. Strain energy for the homogeneous infinite plate with a central crack under pure shear mode.

	360	448	504	588	704	5382
FEM-T3	976.2515	976.2797	976.2868	976.2955	976.3033	976.3471
ES-FEM	976.4103	976.4339	976.4345	976.4363	976.4362	976.4384
Sing ES-FEM	976.5364	976.5639	976.5650	976.5655	976.5660	976.5735

Table 2. K_{II} at point A for the homogeneous infinite plate with a central crack under pure shear mode.

	360 (Error %)	448 (Error %)	504 (Error %)	588 (Error %)	704 (Error %)	5382 (Error %)
FEM-T3	0.9509 (4.9083 %)	0.9625 (3.7461 %)	0.9649 (3.5083 %)	0.9669 (3.3135 %)	0.9710 (2.9042 %)	0.9880 (1.2036 %)
ES-FEM	0.9847 (1.5301 %)	0.9879 (1.2098 %)	0.9894 (1.0580 %)	0.9922 (0.7765 %)	0.9933 (0.6701 %)	0.9937 (0.6287 %)
Sing ES-FEM	0.9888 (1.1155 %)	0.9930 (0.6987 %)	0.9948 (0.5160 %)	0.9970 (0.2958 %)	0.9982 (0.1824 %)	0.9998 (0.0211 %)

Table 3. KII at point B for the homogeneous infinite plate with a central crack under pure shear mode.

	360 (Error %)	448 (Error %)	504 (Error %)	588 (Error %)	704 (Error %)	5382 (Error %)
FEM-T3	0.9628 (3.7221 %)	0.9504 (4.9579 %)	0.9677 (3.2311 %)	0.9654 (3.4580 %)	0.9706 (2.9381 %)	0.9872 (1.2755 %)
ES-FEM	0.9880 (1.1961 %)	0.9847 (1.5292 %)	0.9893 (1.0716 %)	0.9918 (0.8213 %)	0.9928 (0.7172 %)	0.9934 (0.6598 %)
Sing ES-FEM	0.9931 (0.6864 %)	0.9892 (1.0808 %)	0.9944 (0.5577 %)	0.9965 (0.3451 %)	0.9977 (0.2295 %)	0.9997 (0.0285 %)

The analytical formula of the stress intensity factor for such a specimen is given by Tada *et al.* [2000] as:

$$K_{\mathrm{I}} = \sigma\sqrt{\pi a}\left[1.122 - 0.561\left(\frac{a}{w}\right) - 0.205\left(\frac{a}{w}\right)^2 + 0.471\left(\frac{a}{w}\right)^3 - 0.910\left(\frac{a}{w}\right)^4\right] \Big/ \left(1 - \frac{a}{w}\right)^{0.5}. \tag{31}$$

In this example, the parameters used are $w = 4.0\,\mathrm{cm}$, $L = 11.0\,\mathrm{cm}$, $a = 1.2\,\mathrm{cm}$, and $\sigma = 1\,\mathrm{N/cm}^2$. The material is isotropic elastic and material constants are $E = 3\times10^7\,\mathrm{N/cm}^2$ and $\nu = 0.25$. In this example, the effect of increasing the number of S-SD is also examined. The results have been tabulated in Tables 4–6 and depicted in Figs. 14 and 15. Similar to the pervious example, the stress intensity factor behavior has been plotted for one of the crack-tips. Regarding to the results tabulated

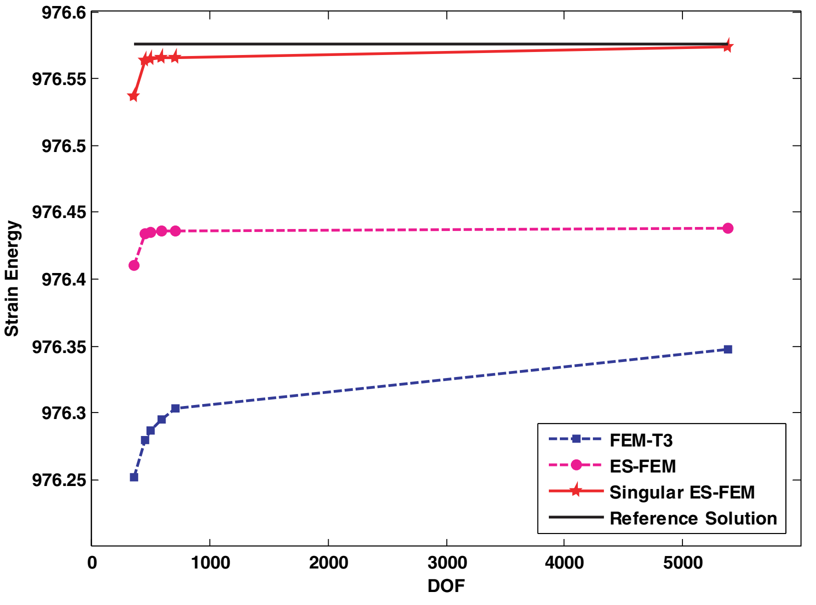

Fig. 11. Strain energy results for the infinite plate under mode II.

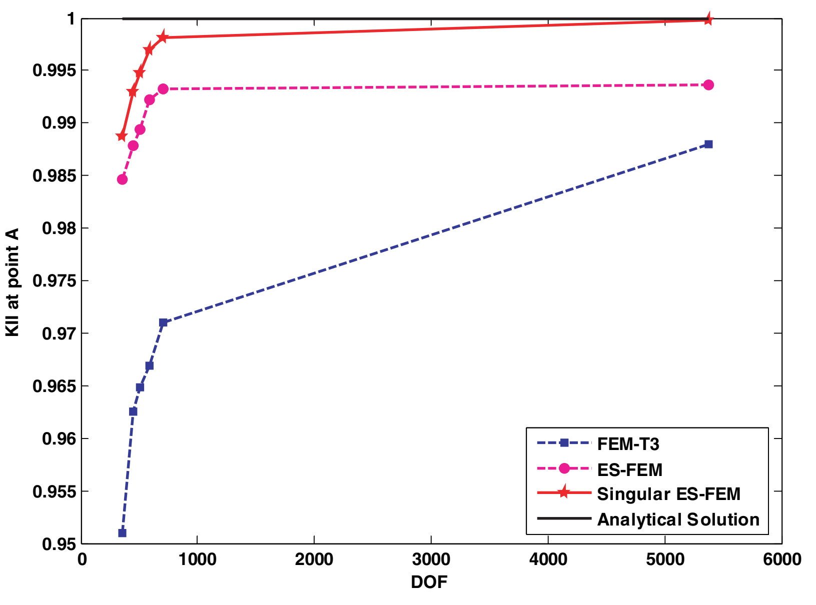

Fig. 12. Normalized stress intensity factor at point A for the infinite plate under mode II.

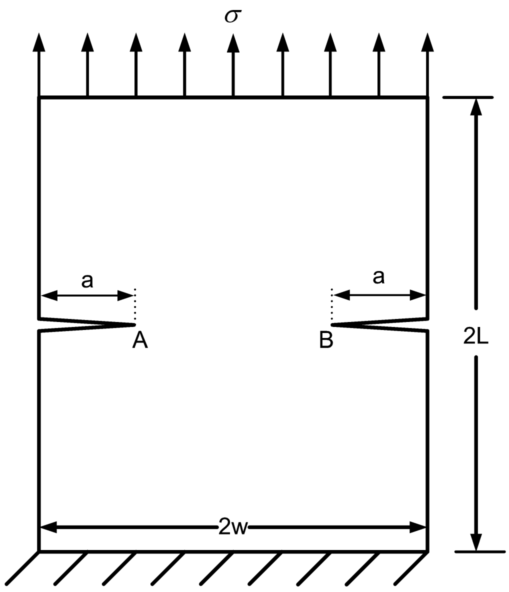

Fig. 13. Double edge crack specimen.

Table 4. Strain energy for double edge crack specimen.

	336	530	948	1286	1780
FEM-T3	2.8552e-004	2.8756e-004	2.8823e-004	2.8860e-004	2.8880e-004
ES-FEM	2.8862e-004	2.8952e-004	2.8960e-004	2.8975e-004	2.8979e-004
Sing ES-FEM (S-SD = 1)	2.8930e-004	2.9022e-004	2.9028e-004	2.9043e-004	2.9047e-004
Sing ES-FEM (S-SD = 2)	2.8953e-004	2.9046e-004	2.9053e-004	2.9068e-004	2.9072e-004

Table 5. K_{I} at point A for double edge crack specimen.

	336 (Error %)	530 (Error %)	948 (Error %)	1286 (Error %)	1780 (Error %)
FEM-T3	0.9249 (7.5073 %)	0.9582 (4.1825 %)	0.9691 (3.0897 %)	0.9722 (2.7782 %)	0.9752 (2.4750 %)
ES-FEM	0.9725 (2.7469 %)	0.9840 (1.5971 %)	0.9843 (1.5716 %)	0.9848 (1.5176 %)	0.9843 (1.5675 %)
Sing ES-FEM (S-SD = 1)	0.9772 (2.2839 %)	0.9890 (1.1035 %)	0.9924 (0.7596 %)	0.9941 (0.5863 %)	0.9985 (0.1498 %)
Sing ES-FEM- (S-SD = 2)	0.9796 (2.0376 %)	0.9916 (0.8378 %)	0.9933 (0.6873 %)	0.9951 (0.4854 %)	0.9994 (0.0564 %)

Table 6. K_I at point B for double edge crack specimen.

	336 (Error %)	530 (Error %)	948 (Error %)	1286 (Error %)	1780 (Error %)
FEM-T3	0.9333 (6.6730 %)	0.9580 (4.2013 %)	0.9715 (2.8513 %)	0.9730 (2.7045 %)	0.9752 (2.4825 %)
ES-FEM	0.9797 (2.0278 %)	0.9826 (1.7409 %)	0.9835 (1.6539 %)	0.9830 (1.6957 %)	0.9842 (1.5832 %)
Sing ES-FEM (S-SD = 1)	0.9844 (1.5616 %)	0.9875 (1.2487 %)	0.9923 (0.7601 %)	0.9931 (0.6845 %)	0.9982 (0.1764 %)
Sing ES-FEM- (S-SD = 2)	0.9868 (1.3239 %)	0.9901 (0.9903 %)	0.9929 (0.7096 %)	0.9945 (0.5476 %)	0.0.9992 (0.0763 %)

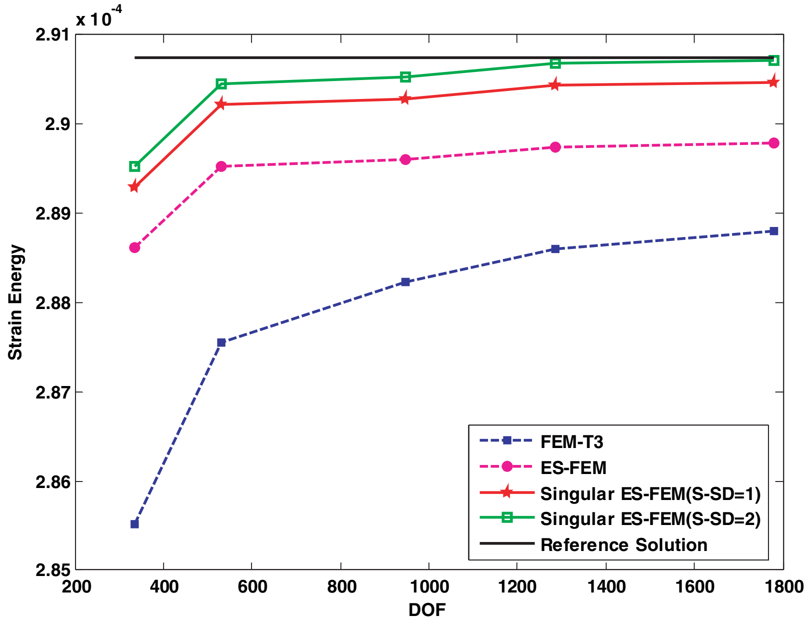

Fig. 14. Strain energy results for the double edge crack specimen.

in the tables it can be seen that the value of stress intensity factor at points A and B is very close to each other.

From these results it can be seen that:

(1) The results of Singular ES-FEM are more accurate than FEM-T3 and standard ES-FEM.
(2) It also can be observed that using two S-SDs (S-SD = 2) can yield to the further improvement in the results including either strain energy and stress intensity factors.

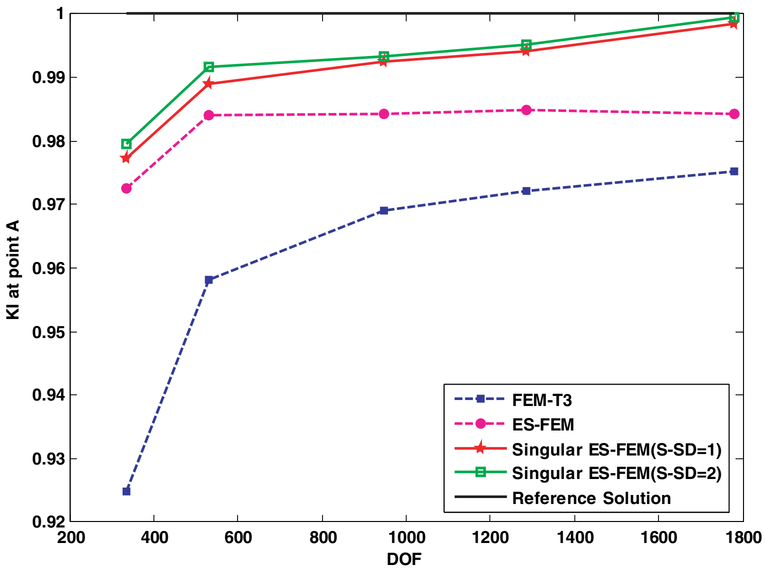

Fig. 15. Normalized K_{I} at point A for the double edge crack specimen.

(3) Based on Tables 5 and 6, it is clear that for this example the value of numerical error for Singular ES-FEM is much less than FEM-T3 and standard ES-FEM. This value decreases more by choosing two S-SDs (S-SD = 2).

3.4. *Homogenous infinite plate with a central inclined crack under mixed mode*

Based on the fact that path independency is the most important feature of the J-integral theory, the stress intensity factors which are calculated in the same fashion presented in Sec. 2.4 should also be path-independent. It means that using the different paths or domains around the crack-tip should not impose a considerable variation in the value of the stress intensity factors. In order to investigate this characteristic for the Singular ES-FEM, an inclined crack under tension load is studied as an example of the mixed-mode situation. This structure is shown in Fig. 16. In this example, $w = 40\,\mathrm{mm}$, $a = \sqrt{2}\,\mathrm{mm}$, $\varphi = \frac{\pi}{4}$, and $\sigma = 1\,\mathrm{MPa}$. The analytical solution for such a structure is available as

$$\begin{cases} K_{\mathrm{I}} = \sigma\sqrt{\pi a}\sin^2\varphi, \\ K_{\mathrm{II}} = \sigma\sqrt{\pi a}\sin\varphi\cos\varphi. \end{cases} \tag{32}$$

For this example φ is fixed as $\varphi = \frac{\pi}{4}$ and therefore we will have

$$\begin{cases} \dfrac{K_I}{\sigma\sqrt{\pi a}} = 0.5000, \\ \dfrac{K_I}{\sigma\sqrt{\pi a}} = 0.5000. \end{cases} \tag{33}$$

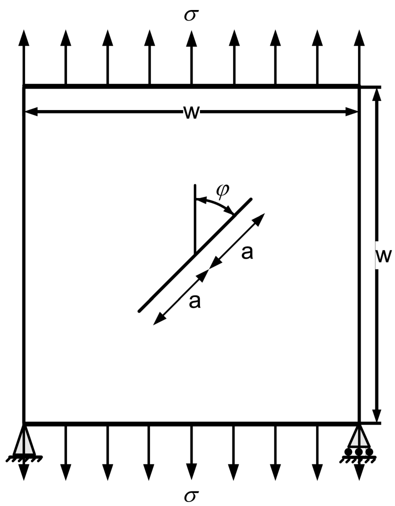

Fig. 16. The plate with an inclined central crack under tension.

The results of stress intensity factors for this structure has been evaluated using Singular ES-FEM with one SD (SD = 1) based on different paths around the crack-tip and outside the crack-tip elements. These results have been tabulated in Tables 7 and 8. Similar to the previous example, it can be clearly observed that Singular ES-FEM presents stable results for different paths chosen around the crack-tip.

Table 7. Path independency at point A for the specimen with inclined crack under tension load.

	$r_d = 0.4$ (Error %)	$r_d = 0.6$ (Error %)	$r_d = 0.7$ (Error %)	$r_d = 0.9$ (Error %)	$r_d = 1$ (Error %)
$\frac{K_{\mathrm{I}}}{\sigma\sqrt{\pi a}}$	0.4991	0.4997	0.4996	0.5001	0.5002
	(0.0867 %)	(0.0269 %)	(0.0359 %)	(0.0127 %)	(0.0203 %)
$\frac{K_{\mathrm{II}}}{\sigma\sqrt{\pi a}}$	0.4962	0.5017	0.5018	0.5060	0.5010
	(0.3799 %)	(0.1685 %)	(0.1804 %)	(0.5965 %)	(0.1050 %)

Table 8. Path independency at point B for the specimen with inclined crack under tension load.

	$r_d = 0.4$ (Error %)	$r_d = 0.6$ (Error %)	$r_d = 0.7$ (Error %)	$r_d = 0.9$ (Error %)	$r_d = 1$ (Error %)
$\frac{K_{\mathrm{I}}}{\sigma\sqrt{\pi a}}$	0.4985	0.4985	0.4987	0.4981	0.4989
	(0.1467 %)	(0.1530 %)	(0.1276 %)	(0.1864 %)	(0.1104 %)
$\frac{K_{\mathrm{II}}}{\sigma\sqrt{\pi a}}$	0.4963	0.5022	0.5022	0.5062	0.5023
	(0.3652 %)	(0.2236 %)	(0.2236 %)	(0.6230 %)	(0.2316 %)

4. Conclusion

In this paper, a general singular ES-FEM has been formulated to evaluate the stress intensity factors for the fracture problems including the domains with more than one crack-tips and under different cases of Mode I, Mode II, or mixed-Mode situation. The method uses the base mesh of linear triangular element which can be generated automatically for complicated geometries. A new five-node triangular element has been formulated and implemented at crack-tip to simulate the stress and strain field singularity. Considering the fact that for the linear elastic fracture mechanics problems, stress intensity factors play the most important role in the crack propagation, this paper tried to focus on stress intensity factors calculation based on Singular ES-FEM. The following points may be drawn from the numerical results.

(1) The singular ES-FEM with one SD (SD = 1) produces converged good results; however, increasing the number of S-SD can somehow improve the results.
(2) The singular ES-FEM has much more accurate results in term of the strain energy in comparison with the standard ES-FEM-T3 and FEM-T3.
(3) The singular ES-FEM has much more accurate results in term of the stress intensity factors in comparison with the standard ES-FEM-T3 and FEM-T3, and works well with the stress intensity factor calculations based on the interact integration.
(4) The numerical results of the singular ES-FEM are stable for different area chosen around the crack-tip and present a very nice "path independency" nature of the stress intensity factors.

References

Chen, J. S., Wu, C. T., Yoon, S. and You, Y. [2000] A stabilized conforming nodal integration for Galerkin meshfree method, *Int. J. Numer. Methods Engin.* **50**, 435–466.

Chen, L., Nguyen-Xuan, H., Nguyen-Thoi, T., Zeng, K. Y. and Wu, S. C. [2009] Assessment of smoothed point interpolation methods for elastic mechanics, *Commun. Numer. Meth. Eng.* doi: 10.1002/cnm.1251.

Dai, K. Y., Liu, G. R. and Nguyen, T. T. [2007] An n-sided polygonal smoothed finite element method (nSFEM) for solid mechanics, *Finite Elem. Anal. Des.* **43**, 847–860.

Dohrmann, C. R., Heinstein, M. W., Jung, J., Key, S. W. and Witkowski, W. R. [2000] Node-based uniform strain elements for three-node triangular and four-node tetrahedral meshes, *Int. J. Numer. Methods Eng.* **47**, 1549–1568.

Li, F. Z., Shih, C. F. and Needleman, A. [1985] A comparison of methods for calculating energy release rates, *Eng. Fract. Mech.* **21**(2), 405–421.

Liu, G. R. [2008] A generalized gradient smoothing technique and the smoothed bilinear form for Galerkin formulation of a wide class of computational methods, *Int. J. Comput. Methods* **5**(2), 199–236.

Liu, G. R. [2009] *Meshfree Methods: Moving Beyond the Finite Element Method*, 2nd Edition (Taylor & Francis/CRC Press, Boca Raton, USA).

Liu, G. R. and Quek, S. S. [2003] *Finite Element Method: A Practical Course* (Butter-worth Heinemann, Burlington, Oxford).

Liu, G. R., Dai, K. Y. and Nguyen, T. T. [2007] A smoothed finite element method for mechanics problems, *Comput. Mech.* **39**, 859–877.

Liu, G. R., Nguyen, T. T. and Lam, K. Y. [2009] An edge-based smoothed finite element method (ES-FEM) for static free and forced vibration analysis, *J. Sound Vibr.* **320**, 1100–1130.

Liu, G. R., Nourbakhshnia, N. and Zhang, Y. W. [2009] A novel singular ES-FEM method for simulating singular stress fields near the crack tips for linear fracture problems, *Eng. Fract. Mech.* doi: 10.1016/j.engfracmech.2009.11.004.

Liu, G. R., Nguyen, T. T., Dai, K. Y. and Lam, K. Y. [2007] Theoretical aspects of the smoothed finite element method (SFEM), *Int. J. Numer. Methods Eng.* **71**, 902–930.

Liu, G. R., Nguyen, T. T., Nguyen, X. H. and Lam, K. Y. [2009c] A node-based smoothed finite element method for upper bound solution to solid problems (NS-FEM), *Comput. Struct.* **87**, 14–26.

Liu, G. R., Zhang, G. Y., Dai, K. Y., Wang, Y. Y., Zhong, Z. H., Li, G. Y. and Han, X. [2005] A linearly conforming point interpolation method (LC-PIM) for 2D solid mechanics problems, *Int. J. Comput. Methods* **2**(4), 645–665.

Nagashima, T. [1999] Node-by-node meshless approach and its applications to structural analyses, *Int. J. Numer. Methods Eng.* **46**, 341–385.

Puso, M. A. and Solberg, J. [2006] A stabilized nodally integrated tetrahedral, *Int. J. Numer. Methods Eng.* **67**, 841–867.

Puso, M. A., Chen, J. S., Zywicz, E. and Elmer, W. [2008] Meshfree and finite element nodal integration methods, *Int. J. Numer. Methods Eng.* **74**, 416–446.

Rice, J. R. [1968] A path independent integral and the approximate analysis of strain concentration by notches and cracks, *J. Appl. Mech.* **35**, 379–386.

Shih, C. and Asaro, R. [1985] Elastic-plastic analysis of cracks on bimaterial interfaces: Part I — small scale yielding. *J. Appl. Mech.* **55**, 299–316.

Tada, H., Paris, P. C. and Irwin, G. R. [2000] *The Stress Analysis of Cracks Handbook* (ASME Press, New York).

Yau, J., Wang, S. and Corten, H. [1980] A mixed mode crack analysis of isotropic solids using conservation laws of elasticity, *J. Appl. Mech.* **47**, 335–341.

Yoo, J. W., Moran, B. and Chen, J. W. [2004] Stabilized conforming nodal integration in the natural-element method, *Int. J. Numer. Methods Eng.* **60**, 861–890.

Zienkiewicz, O. C. and Taylor, R. L. [2000] *The Finite Element Method*, 5th edition (Butterworth Heinemann, Oxford).